ISSN 1070-4272, Russian Journal of Applied Chemistry, 2018, Vol. 91, No. 11, pp. 1821−1829. © Pleiades Publishing, Ltd., 2018.
Original Russian Text © E.E. Knyazeva, I.V. Dobryakova, A.V. Shkuropatov, O.A. Ponomareva, Yu.G. Kolyagin, I. I. Ivanova, 2018, published in Zhurnal Prikladnoi Khimii, 2018, Vol. 91, No. 11, pp. 1610−1619.

TECHNOLOGICAL PRODUCTION OF NEW MATERIALS

Influence of Synthesis Conditions on Properties of MWW Zeolites

E. E. Knyazeva[a,b,*], I. V. Dobryakova[a], A. V. Shkuropatov[a], O. A. Ponomareva[a,b], Yu. G. Kolyagin[a], and I. I. Ivanova[a,b]

Lomonosov Moscow State University, Moscow, 119991 Russia
Topchiev Institute of Petrochemical Synthesis, Russian Academy of Sciences, Moscow, 119991 Russia
**e-mail: eknyazeva62@mail.ru*

Received October 12, 2018

Abstract—The influence of the preparation conditions on the physicochemical properties of zeolite MWW at varying the type of source of SiO_2, the concentration parameters of the reaction mixture, temperature and duration of crystallization. The synthesis conditions providing a high degree of utilization of inorganic sources of raw materials and an MWW zeolite yield of 96% were determined. It was shown that performing the crystallization at 150°C results in that uniform-size crystals of MWW zeolite are formed. The concentrating limits of the reaction mixture were determined, at which a pure-phase MWW zeolite with pore volume of 0.33–0.34 $cm^3\ g^{-1}$ and micropore volume of 0.17–0.18 $cm^3\ g^{-1}$ can be obtained.

Keywords: MWW zeolite, synthesis conditions, crystallization product

DOI: 10.1134/S1070427218110125

Ethylbenzene and isopropylbenzene (cumene) are key half-products of petrochemical synthesis and raw materials for obtaining monomers from which modern polymers, resins, and plastics are manufactured. The synthesis of ethylbenzene and cumene is based on the process of benzene alkylation with lower olefins in the presence of an acid catalyst. The most promising catalysts for the alkylation of benzene with olefins are zeolites of several structural types, including MFI, FAU, BEA, and MWW. Among the above structures, the attention of researchers working in this field has been attracted in recent years by MWW zeolite. Catalysts based on this zeolite are characterized by greater selectivity, low oligomerizing ability and high stability ensuring long catalyst life of several years [1]. Specific features of the catalytic effect of MWW zeolite are due to the specificity of its crystal and porous structure, morphology of the crystals, and acidity.

Zeolite MWW has a unique porous structure, which differs from other zeolites by the method of spatial organization, which is carried out by the aggregation of 2.5 nm thick layers supercell with the size [2]. The layer is constructed on the basis of a so-called 1.64 × 1.82 nm. A layered precursor is formed during a hydrothermal synthesis of MWW zeolite. In the precursor, the space between the layers is filled by molecules of the template hexamethyleneimine (HMI) [2]. The layers are covered by silanol groups and are retained near each other via hydrogen bonds with template molecules. When calcining the precursor to remove the template as a result of the reaction of dehydration, the Si–OH bonds on the surface of the layers interact with each other the formation of siloxane bonds Si–O–Si. As a result, the interlayer space becomes narrower and the crystal structure is densified. Crystals of MWW zeolite have the shape of a disk up to 1.5 μm in size with a thickness of about 100 nm. The disks are aggregated into formations of various shapes: spheres [3], torus rings [4], and rosettes [5].

The microporous structure of MWW zeolite is formed by two independent systems of pores [6]. The first system includes half-hollows 7 × 7 × 7 Å in size, connected with each other via windows delimited by 10-member silicon-oxygen rings. The half-hollows are predominantly localized on the outer surface of planar crystallites in the

form of a disk. The second system of pores has the form of sinusoidal channels situated in parallel to the disk plane, delimited by 10-member ring and not connected with each other [7]. Aluminum atoms in the crystal structure of the MWW zeolite and, accordingly, acid centers are localized predominantly in the half-cavities, this ensures the presence of strong Brönsted acid sites on the outer surface [8]. This is the difference of MWW zeolite from zeolites of other structural types in which strong acid centers are located in the bulk of the zeolite crystal.

In the last decade, the researchers' attention has been associated with the synthesis and study of properties of hierarchical zeolites of the MWW family, which obtained by the methods of pillaring, peeling [9, 10], silanization [11], and recrystallization [12]. At the same time, no clear regularity has been established of the influence of the synthesis conditions on the morphological and textural properties of MWW zeolite and its layered precursor. Analysis of publications concerned with the synthesis of MWW zeolite shows that most of research teams work within a very narrow range of qualitative and quantitative compositions of reaction mixtures crystallizing into MWW zeolite. Most frequently aerosil is used as a source of SiO_2 [13, 14]. The reaction mixtures are characterized by SiO_2/Al_2O_3 ratio from 30 to 50, high concentration of HMI template ($HMI/SiO_2 = 0.35–0.60$) and high dilution ($H_2O/SiO_2 = 35–45$) [5, 15]. In the literature there are no data on the influence of synthesis conditions, including temperature, duration, and mixing, on the yield of the crystalline phase of the MWW zeolite, which is one of fundamental importance when deciding how to organize the production of this zeolite.

The issues of regulating the structural, morphological, and textural properties of zeolite MWW under various conditions of synthesis, as well as the assessment of its quantitative yield during hydrothermal crystallization, are the subject of this article.

EXPERIMENTAL

The composition of the reaction mixture from [13, 16] was chosen as the base. The reaction mixture of composition $0.09Na_2O·0.033Al_2O_3·SiO_2·0.5HMI·45H_2O$ was prepared from calculated amounts of aerosil or silica gel, sodium aluminate, sodium hydroxide, hexamethyleneimine, and water. As varied synthesis parameters were chosen the type of the SiO_2 source [aerosil (EVONIK Industries) and silica gel (KSKG brand], H_2O/SiO_2 molar ratio in the reaction mixture (15–45), synthesis temperature (150 and 170°C), crystallization duration (3–7 days), and application of rotation. The crystallization was performed in autoclaves with external heating. To evaluate the reproducibility of MWW zeolite synthesis and characteristics and yield of the zeolite, the crystallization was performed in 150- and 1000-mL autoclaves. After the crystallization was complete, the solid product was separated, washed on a filter, dried at 100°C for 12 h, and calcined to remove the template at 550°C for 12 h.

XRD analysis of the samples was based on diffraction patterns obtained on a Bruker D2 PHASER diffractometer with CuK_α radiation at 2θ angles of 5–40° with a step of 0.05° at slit width of 1 mm and recording duration at a point of 3 s.

MAS NMR spectra on ^{27}Al nuclei were obtained on a VARIAN Unity Inova AS-500 instrument. The chemical shift of ^{27}Al was calibrated relative to $Al(NO_3)_3$.

The chemical composition of MWW zeolites was determined by XRF analysis on a Thermo Scientific ARL Perform instrument with a 3.5-kW rhodium tube. Prior to an analysis, 0.15–0.20-g weighed portions of samples were compacted into pellets with boric acid.

The yield of the zeolite phase (in per cent relative to the theoretical value) was calculated by the formula

$$Y = [m_{zeol}\omega(SiO_2) + m_{zeol}\omega(Al_2O_3)]/[m_{RM}(SiO_2) + m_{RM}(Al_2O_3)] \times 100\%,$$

where m_{zeol} is the mass of the resulting zeolite; $\omega(SiO_2)$ and $\omega(Al_2O_3)$, mass fractions of SiO_2 and Al_2O_3 in the zeolite according to the results of a chemical analysis; and $m_{RM}(SiO_2)$ and $m_{RM}(Al_2O_3)$, masses of SiO_2 and Al_2O_3 in the reaction mixture.

SEM images of the samples were obtained on a Hitachi TM3030 microscope. Prior to the measurements, a layer of gold was deposited onto the sample surface via evaporation in a vacuum.

The porous structure characteristics were determined by the method of low-temperature adsorption of nitrogen. Isotherms were measured by the standard procedure on a Micromeritics ASAP 2010 porosimeter. The porous structure characteristics were calculated by the software package shipped with the instrument.

The acid properties were examined by the method of temperature-programmed desorption (TPD) of

Synthesis conditions and characteristics of the products formed in crystallization of the reaction mixture of composition $0.09Na_2O{\cdot}0.033Al_2O_3{\cdot}0.5HMI{\cdot}SiO_2{\cdot}(15–45)H_2O$

Sample	Synthesis conditions					Properties of crystallization products				
	source of SiO_2	H_2O/SiO_2, mol/mol	crystallization conditions			phase composition	Si/Al, mol/mol	micropore volume, $cm^3\ g^{-1}$	pore volume, $cm^3\ g^{-1}$	yield, %
			T, °C	τ, days	rotation					
MWW-1	Aerosil	45	170	7	+	MWW + MFI	11.7	0.12	0.19	72
MWW-2	"	45	150	7	+	MWW	13.5	0.19	0.31	80
MWW-3	"	35	150	7	+	MWW	13.7	0.19	0.32	84
MWW-4	Silica gel	35	150	7	+	MWW	13.4	0.17	0.32	80
MWW-5	"	35	150	7	-	MWW	13.0	0.18	0.28	77
MWW-6	"	25	150	7	+	MWW	13.2	0.18	0.33	96
MWW-7	"	20	150	7	+	MWW + MFI	n/d	0.14	0.30	94
MWW-8	"	15	150	7	+	MWW + MFI + MOR	n/d	0.13	0.28	94
MWW-9	"	35	150	5	+	MWW	12.4	0.18	0.34	77
MWW-10	"	35	150	3	+	MWW	10.5	0.16	0.28	55
MWW-11	"	35	150	5	+	MWW	12.5	0.17	0.33	82
MWW-12	"	25	150	5	+	MWW	12.7	0.17	0.32	93

ammonia. Experiments were performed on USGA-101 chemisorption analyzer manufactured by UNISIT (Russia). A 0.15–0.20-g portion of a sample was placed in a tubular quartz reactor. The standard automated pretreatment included successive stages of sample calcination at 500°C for 1 h in a flow of helium, saturation with ammonia at a temperature of 60°C for 15 min, and removal of physically adsorbed ammonia in a flow of helium at 100°C. The experiment on TPD of NH_3 was performed in a flow of helium (30 mL min^{-1}), with temperature raised at a rate of 8 deg min^{-1} and released ammonia recorded with a heat-conductivity detector.

RESULTS AND DISCUSSION

The synthesis conditions of MWW zeolite samples and the properties of the crystallization products are presented in the table.

The crystallization at 170°C of the reaction mixture with base composition, prepared on the basis of aerosil (see the table, MWW-1 sample), resulted in that an MWW zeolite was formed with an admixture of MFI zeolite. In the diffraction pattern of MWW-1 sample (Fig. 1a), the reflection corresponding to the MFI phase is denoted by the asterisk. A SEM image of sample MWW-1 shows (Fig. 2a) that the zeolite was formed as planar crystals with sizes of 0.5–3.0 μm, aggregated into rosettes about 6 μm in size. Wide size distribution of primary planar crystals may be due to the specific features of the source of SiO_2, aerosil—highly dispersed form of silicon oxide, formed by dense nonporous silicon oxide particles with sizes of 300–400 μm. The initial stages of crystallization of the reaction mixtures based on aerosil are associated with the occurrence of parallel-sequential process in which nonporous aerosil particles are dissolved (only on the outer surface of the particles) and dissolution products are condensed to give secondary building units forming a basis for the construction of the skeleton of the zeolite. As a result of the prolonged dissolution of aerosil, fluctuations may appear in the volume of the reaction mixture, which gives crystals of different sizes.

The data in the table show that the volumes of pores and micropores in sample MWW-1 are 0.19 and 0.12 $cm^3\ g^{-1}$, respectively. The type of isotherm of nitrogen adsorption for the material obtained (Fig. 3) is typical of MWW zeolite [10, 17]. The isotherm exhibits a

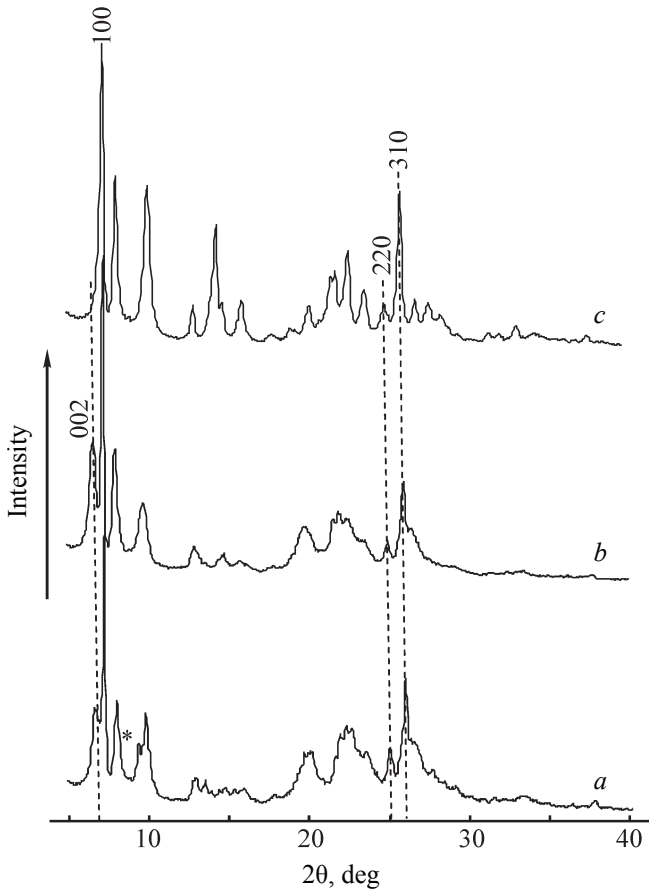

Fig. 1. Diffraction patterns of samples. (*a*) MWW-1, not calcined; (*b*) MWW-2, not calcined; (*c*) MWW-2, calcined.

steep rise at $p/p_0 > 0.9$, which corresponds to aggregation of coarse particles.

Lowering the crystallization temperature of the base reaction mixture from 170 to 150°C (see the table, sample MWW-2) resulted in a significant change in the properties of the zeolite material. At 150°C, the reaction mixture crystallized to give a phase-pure MWW zeolite (Fig. 1b) having the form of planar plate-like aggregates 1.5–2.0 μm in size (Fig. 2b).

The diffraction pattern of a freshly synthesized sample MWW-2, which contains the HMI template and has the form of a layered precursor of MWW zeolite, shows a reflection with *hkl* 002. This reflection corresponds to the presence of 2.5-nm-thick individual layers of MWW zeolite (Fig. 1b) [17]. The reflections with *hkl* = 100, 220, and 310 (Fig. 1b) correspond to the crystal structure within the layer. Calcination of sample MWW-2 led to disappearance of the reflection with *hkl* = 002 (Fig. 1c). This indicated that the layers interact to give an extended bulk structure, with the crystal structure of the primary layer preserved. The formation of the bulk structure of MWW zeolite was accompanied by a distinct resolution of diffraction peaks at 2θ = 19.8–24.3° (Fig. 1c).

According to the classical concept of zeolite crystallization, lowering the synthesis temperature must lead to a slower crystallization rate. However, during the same synthesis duration (7 days), the volumes of pores and micropores in sample MWW-2 substantially exceed the same values for sample MWW-1 (see the table). The observed differences suggest that at a crystallization temperature of 170°C, the synthesis time of 7 days (determined from literature data) is much longer than the time required to achieve maximum crystallinity.Probably, by the end of the synthesis of the MWW-1 sample at 170°C, the processes of destruction of the formed zeolite phase already occurred in the reaction mixture. The broad crystal size distribution in sample MWW-1 may be due not only to the specific features of the raw-material source of SiO_2 (as described above), but also to the corrosive effect of the alkaline synthesis medium. As additional evidence of the weaker effect of corrosion in the synthesis of sample MWW-2 at 150°C serve the higher yield of the zeolite phase in sample MWW-2, compared with sample MWW-1 (see the table, 80 and 72%, respectively) and the increase in the Si/Al ratio, which was for MWW-1 and MWW-2 11.7 and 13.5, respectively (see the table).

The technique of concentrating the reaction mixture is used as a way to increase the productivity of reactors for the synthesis of zeolites. It can be seen in the table that lowering the H_2O/SiO_2 molar ratio in the reaction mixture from 45 (sample MWW-2) to 35 (sample MWW-3) led to an increase in the yield of the zeolite from 80 to 84%. The rise in the yield of the zeolite was associated with an insignificant increase in the Si/Al ratio from 13.5 to 13.7 (see the table), rather than with a change in the phase composition, morphology of crystals, and porous-structure characteristics. Further concentration of reaction mixtures was difficult. This is due to the impossibility of homogenization of aerosil-based mixtures with ratios H_2O/SiO_2 <30 due to their high viscosity.

The replacement of aerosil as the source of SiO_2 with a silica gel with a developed mesoporous structure with pores having diameter of 10–12 nm led to a change of the morphology of MWW zeolite crystals. As shows a SEM image of sample MWW-4 (Fig. 2c) the crystallization of a reaction mixture based on silica gel under the conditions similar to those for sample MWW-3 (yielded a zeolite

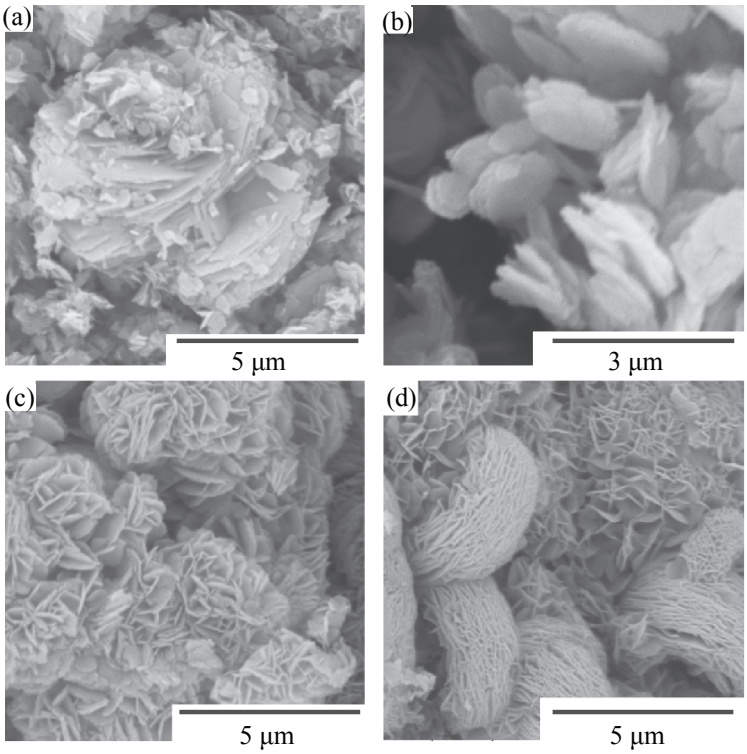

Fig. 2. SEM micrographs of samples (a) MWW-1, (b) MWW-2, (c) MWW-4, (d) MWW-5.

material) of an openwork spatial grid of flat elliptical crystals 1.0–1.5 μm in size and 100 nm thick). The change of the raw-material source did not lead to a substantial change in the porous-structure characteristics of the zeolite and its chemical composition. The Si/Al ratio in sample MWW-4 was 13.4 (see the table).

Performing a similar synthesis without rotation (see the table, sample MWW-5) favored an inhomogeneity of the reaction mixture, which yielded aggregates in the form of torus rings distributed in a network of planar crystals (Fig. 2d).

Using silica gel as a source of SiO_2 was accompanied by a decrease in the yield of the zeolite, compared with sample MWW-3 to 80 and 77% for samples MWW-4 and MWW-5, respectively. To determine the possibility of controlling the yield of the zeolite phase under the conditions of concentrated reaction mixture (all other synthesis conditions being the same as those for sample MWW-4), we obtained samples MWW-6, MWW-7, and MWW-8, for which the H_2O/SiO_2 molar ratio in the reaction mixture was 25, 20, and 15, respectively. The data in the table demonstrate that raising the concentration of dry substance in the reaction mixture favored an increase in the yield of the zeolite phase to 94–96%. In this case, lowering the H_2O/SiO_2 ratio in the reaction mixture from 35 (sample MWW-4) to 25 (sample MWW-6) did not change the phase and chemical composition, texture of the material and morphology of MWW zeolite crystals (see the table). At the same time, concentration of the reaction mixture to H_2O/SiO_2 ratios of 20 and 15 resulted in that dense plate-like (Fig. 4a, sample MWW-

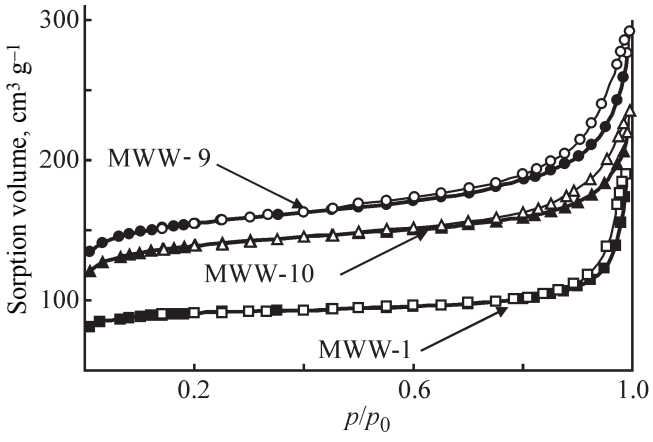

Fig. 3. Isotherms of low-temperature adsorption–desorption of nitrogen on samples of MWW zeolite.

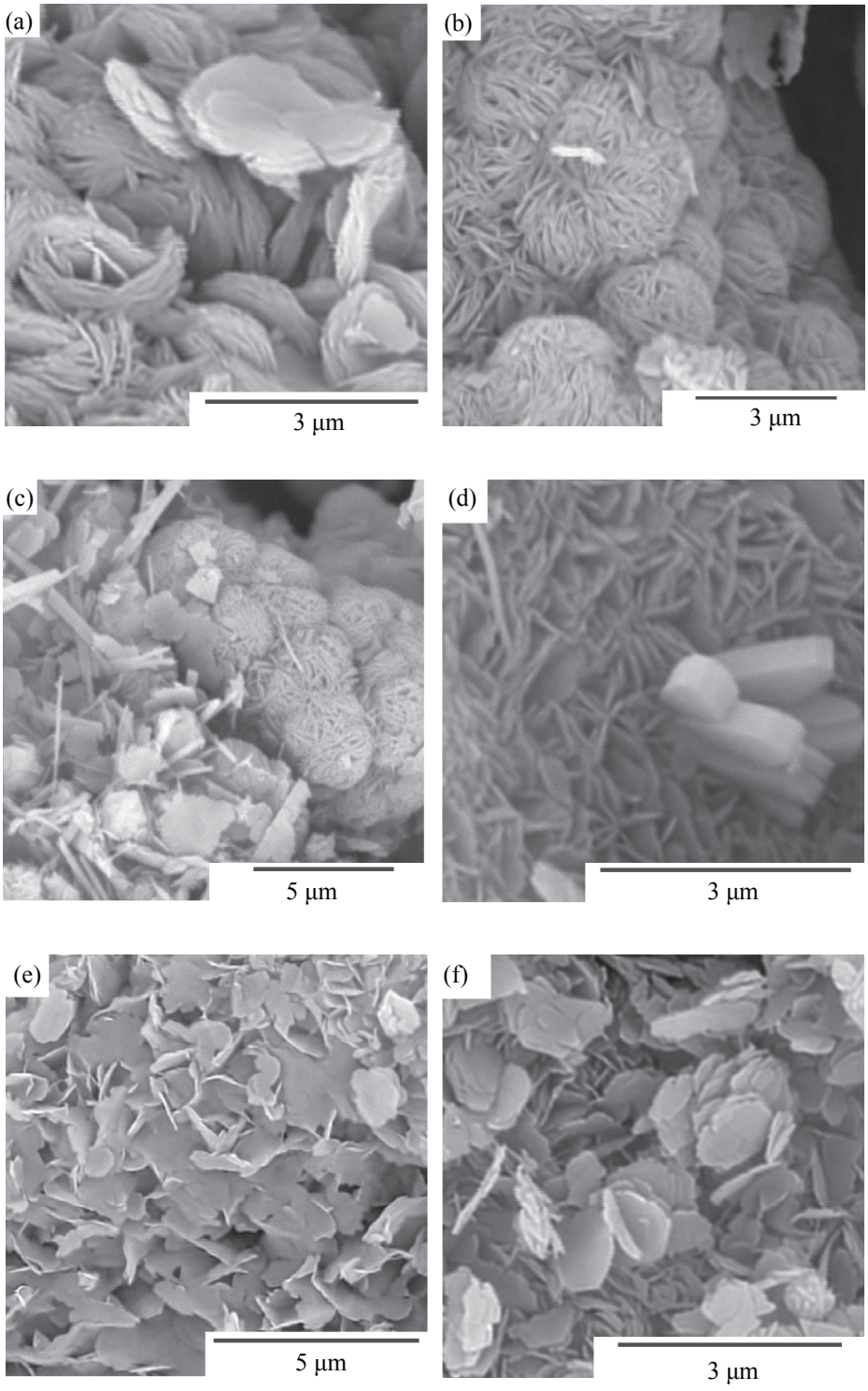

Fig. 4. SEM micrographs of samples (a) MWW-7, (b–d) MWW-8, (e) MWW-11, (f) MWW-12.

7) and spherical (Fig. 4b, sample MWW-8) aggregates. The crystallization of a reaction mixture with H_2O/SiO_2 ratio of 20 (sample MWW-7) was accompanied by the formation of an admixture of MFI zeolite (see the table). Lowering the H_2O/SiO_2 ratio to 15 favored the formation of admixtures of MFI and MOR zeolites. The presence of these in sample MWW-8 was recorded both in the diffraction patterns and in SEM micrographs

of a sample (Fig. 4c, acicular MOR crystals and Fig. 4d, prismatic MFI crystals). Thus, for reaction mixtures based on silica gel, there is the optimal range of dry-substance concentrations at H_2O/SiO_2 ratios in the range 25–35, which provides the phase purity of MWW zeolite.

Information on the kinetic aspects of the crystallization of the MWW zeolite and the processes accompanying the formation of this zeolite phase during the synthesis is practically absent in the specialized literature. We traced the evolution of the solid phase and changes in the properties of the material in the course of crystallization for the example of samples MWW-10, MWW-9, and MWW-4 synthesized under identical conditions with crystallization durations of 3, 5, and 7 days, respectively (see the table). It follows from the data in the table that the formation of the crystal structure of MWW at synthesis durations of 3–7 days is not accompanied by formation of other crystalline phases. The morphology of crystals remains unchanged within this range, all the samples have the form of openwork spatial grid of flat elliptical crystals (Fig. 2c) whose size increases from 0.6–1.0 μm for sample MWW-10 (synthesis during 3 days) to 1.0–1.5 μm for sample MWW-4 (synthesis for 7 days). Sample MWW-10 with the shortest synthesis duration of 3 days is already a highly crystalline material with micropore volume of 0.16 $cm^3\ g^{-1}$ (see the table).

Raising the crystallization duration from 3 to 5 days does not change the run of the isotherms for samples MWW-10 and MWW-9 (Fig. 3). The increase in the pore volume in sample MWW-9 to 0.34 $cm^3\ g^{-1}$, which occurs due to mesopores, is evidenced in the isotherms by the steeper rise in an isotherm at $p/p_0 > 9$. The insignificant differences between the porous-structure characteristics of samples MWW-9 and MWW-4 (see the table) show that the porous structure of MWW zeolite is fully formed already after 5 days of crystallization.

A chemical analysis of samples MWW-10, MWW-9, and MWW-4 demonstrated that an increase in the synthesis duration is accompanied by a rise in the Si/Al ratio from 10.5 to 13.4. In this case, the yield of the zeolite increased from 55 to 80% (see the table). The changes in the chemical composition of the samples indicate that the gain in the zeolite phase during the synthesis of MWW zeolite apparently occurs due to silicon present in the liquid phase.

We evaluated the effect of synthesis scaling on the properties of the MWW zeolite using the example of sample MWW-9. For this purpose, we obtained sample MWW-11 under the conditions similar to those for sample MWW-9. This sample was crystallized in the 1-L autoclave, with the weighed portions of the starting reagents accordingly corrected. As follows from the characteristics of sample MWW-11 in the table, a high reproducibility of all the properties of sample MWW-9 was reached under the scaling conditions. SEM images of sample MWW-11 (Fig. 4e) demonstrate that the zeolite was crystallized as openwork spatial grid of flat elliptical plate-like crystals with sizes not exceeding 1.5 μm. To raise the yield of MWW zeolite, equal to 82% for sample MWW-11 (see the table), we concentrated the reaction mixture to $H_2O/SiO_2 = 25$ and obtained sample MWW-12. As the data in the table show, the yield of zeolite during the synthesis of the MWW-12 sample was increased to 93% while maintaining the phase, chemical composition, and characteristics of the porous structure. SEM images of sample MWW-12 (Fig. 4f) show that synthesis from a more concentrated reaction mixture yields separate elliptical plate-like crystals with sizes of 1.0–1.5 μm and thickness of about 100 nm, rather than openwork spatial grid.

The acid form of MWW zeolite, used as an alkylation catalyst, is obtained in standard successive procedures of crystallization, washing, drying to remove the template and performing an ion exchange in an ammonium salt solution, with the subsequent calcination to decompose the ammonium cation. The ^{27}Al NMR spectra in Fig. 5 made it possible to find for the example of sample MWW-11 how the state of aluminum changes in the course of post-synthesis treatments. It follows from the ^{27}Al NMR spectrum in Fig. 5a that, after being synthesized, sample MWW-11 contains aluminum exclusively in tetrahedral positions of the skeleton. This is evidenced by the presence of an asymmetric signal, which is a superposition of signals at about 55.5 and 49 ppm. According to [18], the signal at about 55.5 ppm corresponded to aluminum present on the outer surface and in supercells of MWW zeolite, at the signal at about 49.0 ppm, with that in pockets and sinusoidal channels. Calcination of the sample to remove the template is accompanied by the appearance in the NMR spectrum of a signal at about –0.4 ppm (Fig. 5b), which indicates that extra-framework aluminum is formed. The ion exchange in an ammonium nitrate solution leads to the disappearance of this signal (Fig. 5c). The fact that the Si/Al ratios in the sodium and ammonium forms of sample MWW-11 are very close (12.5 and 12.4, respectively)

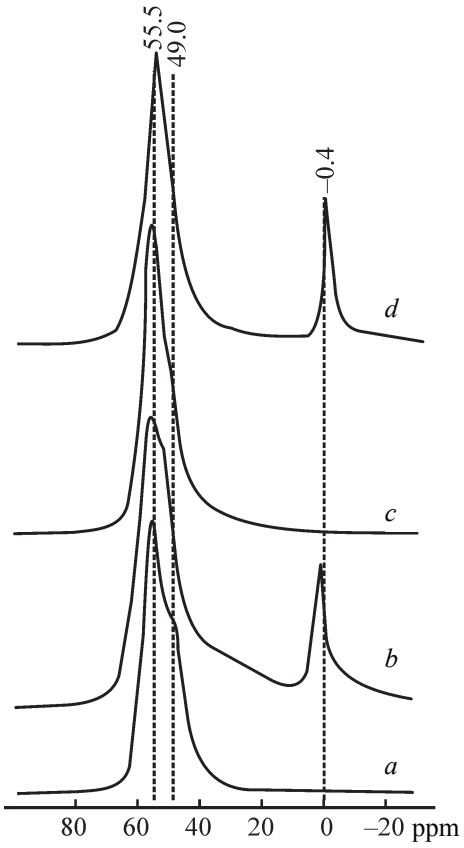

Fig. 5. 27Al NMR spectra of samples. (*a*) MWW-11, not calcined; (*b*) MWW-11, calcined; (*c*) NH4-MWW-11; (d) H-MWW-11.

may indicate that the extra-framework aluminum is incorporated into the crystalline skeleton in the course of the ions exchange, but this assumption invites a special study. Calcination of the ammonium form of sample MWW-6 to give the hydrogen form of the zeolite again yielded extra-framework aluminum, which was evidenced by the appearance in the NMR spectrum of the signal at about –0.4 ppm (Fig. 5d). Thus, aluminum is present in the hydrogen form of MWW zeolite in two states: in tetrahedral positions of the crystalline skeleton, which are responsible for the Brønsted acidity of MWW zeolite, and extra-framework positions of the skeleton.

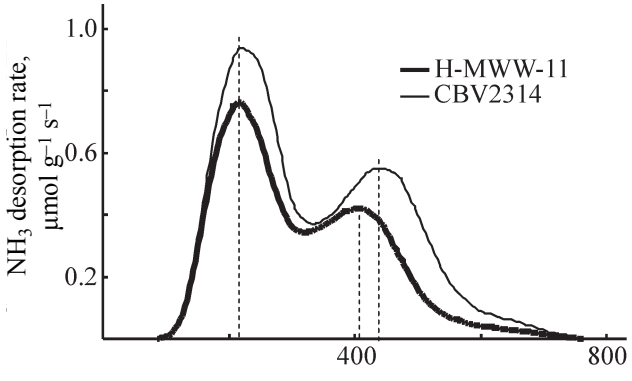

Fig. 6. NH_3 TPD spectra of zeolites.

The acidic properties of the hydrogen form of sample MWW-11 were examined by the method of TPD and compared with the properties of an industrial sample of ammonia of MFI zeolite with same chemical composition (Zeolyst, lot CBV2314). The concentrations of acidic centers in H-MWW-11 and H-CBV2314 were 1150 and 1370 μmol g^{-1}, respectively. The NH_3 TPD spectra of both samples (Fig. 6) show two peaks corresponding to the presence in the zeolites of acidic centers with different strengths: weak centers to which corresponds the thermal desorption peak at around 220°C, and strong centers, with a thermal desorption peak at a temperature exceeding 400°C. The coincidence for samples H-MWW-11 and H-CBV2314 of the positions of the peaks corresponding to weak acid centers indicates that their weak acidities are of the same nature. The positions of the peaks corresponding to strong cid centers differ by 30° for MWW and MFI zeolites; being 415°C for sample H-MWW-11 and 445°C for sample H-CBV2314. The results obtained are in full agreement with published data, according to which MWW zeolite is inferior in strength of acid centers to other high-silica zeolites.

CONCLUSIONS

Trom the results presented in the communication showed that the morphological and texture characteristics of MWW zeolite can be controlled by varying the crystallization temperature and sources of raw materials and concentrating the reaction mixture. The crystallization temperature of 150°C provides a homogeneous size distribution of crystallites of MWW zeolite. Use of silica gel as a source of SiO_2 makes it possible to obtain MWW zeolite as openwork spatial network formed by planar crystals with sizes not exceeding 1.5 μm and thickness of 100 nm. Lowering the H_2O/SiO_2 molar ratio in the reaction mixture to 25 leads to an increase in the yield of the zeolite to 93–96% and ensures a high completeness of utilization of the starting inorganic raw material. Further concentration of the reaction mixtures changes the crystallization selectivity and results in that admixture crystalline phases of MOR and MFI zeolites are formed.

ACKNOWLEDGMENTS

This work was financially supported by the Ministry of Education and Science of the Russian Federation (unique applied research identifier RFMEFI60717X0167).

REFERENCES

1. Degnan, T.F., Smith, C.M., and Venkat, C.R., *Appl. Catal. A*, 2001, vol. 221, nos. 1–2, pp. 283–294.
2. Díaz, U. and Corma, A., *Dalton Trans*., 2014, vol. 43, pp. 10292–10316.
3. Kumar, Sh., Pusparatu, S., Komura, K., Kubota, Y., and Sugi, Y., *Mater. Trans., Spec. Issue*, 2005, vol. 46, no. 12, pp. 2651–2658.
4. Liu, Z., Shen, S., Tian, B., Sun, J., Tu, B., and Zhao, D., *Chin. Sci. Bull*., 2004, vol. 49, no. 6, pp. 556–561.
5. Wu, Y., Ren, X., Lu, Y., and Wang, J., *Microporous Mesoporous Mater*., 2008, vol. 112, nos. 1–3, pp. 138–146.
6. Leonowicz, M.E., Lawton, J.A., Lawton, S.L., and Rubin, M.K., *Science*, 1994, vol. 264, pp. 1910–1913.
7. Juttu, G.G. and Lobo, R.F., *Microporous Mesoporous Mater*., 2000, vol. 40, no. 1, pp. 9–23.
8. Li, Y., Guo, W., Fan, W., and Yuan, S., *J. Mol. Catal. A: Chem*., 2011, vol. 338, nos. 1–2, pp. 24–32.
9. Corma, A., Fornes, V., Pergher, S.B., Maesen, Th.L.M., and Buglass, J.G., *Nature,* 1998, vol. 396, no. 26, pp. 353–356.
10. Corma, A., Fornés, V., Guil, J.M., Pergher, S., Maesen, Th.L.M., and Buglass, J.G., *Microporous Mesoporous Mater.*, 2000, vol. 38, no. 23, pp. 301–309.
11. Wu, P., Ruan, J., Wang, L., Wu, L., Wang, Y., Liu, Y., Fan, W., He, M., Terasaki, O., and Tatsumi, T.J., *Am. Chem. Soc.*, 2008, vol. 130, pp. 8178–8187.
12. Song, K., Guan, J., Wu, S., Yang, Y., Liu, B., and Kan, Q., *Catal. Lett.*, 2008, vol. 126, nos. 3–4, pp. 333–340.
13. Dıáz, U., Fornes, V., and Corma, A., *Microporous Mesoporous Mater.,* 2006, vol. 90, nos. 1–3, pp. 73–80.
14. Corma, A., Corell, C., and Pérez-Pariente, J., *Zeolites*, 1995, vol. 15, no. 1, pp. 2–8.
15. Cheng, M., Tan, D., Liu, X., and Han, X., *Microporous Mesoporous Mater.*, 2001, vol. 42, nos. 2–3, pp. 307–316.
16. Güray, I., Warzywoda, J., Bac, N., and Sacco, A., *Microporous Mesoporous Mater*., 1999, vol. 31, no. 3, pp. 241–251.
17. Schwanke, A.J., Pergher, S., Díaz, U., and Corma, A., *Microporous Mesoporous Mater*., 2017, vol. 254, no. 1, pp. 17–27.
18. Wang, Y., Gao, Y., Xie, S., Liu, Sh., Chen, F., Xin, W., Zhu, X., Li, X., Jiang, N., and Xu, L., *Catal. Today,* 2018, vol. 316, pp. 71–77.